

Control-matrix approach to stellarator design and control

H. E. Mynick and N. Pomphrey

Plasma Physics Laboratory, Princeton University, P.O. Box 451, Princeton, New Jersey 08543-0451

(Received 31 January 2000; accepted 17 August 2000)

The full space $\mathbf{Z} \equiv \{Z_j = 1, \dots, N_z\}$ of independent variables defining a stellarator configuration is large. To find attractive design points in this space, or to understand operational flexibility about a given design point, one needs insight into the topography in \mathbf{Z} -space of the physics figures of merit P_i which characterize the machine performance, and means of determining those directions in \mathbf{Z} -space which give one independent control over the P_i , as well as those which affect none of them, and so are available for design flexibility. The control matrix (CM) approach described here provides a mathematical means of obtaining these. In this work, the CM approach is described and used in studying some candidate Quasi-Axisymmetric (QA) stellarator configurations the National Compact Stellarator Experiment design group has been considering. In the process of the analysis, a first exploration of the topography of the configuration space in the vicinity of these candidate systems has been performed, whose character is discussed. © 2000 American Institute of Physics.
[S1070-664X(00)00912-5]

I. INTRODUCTION

The full space $\mathbf{Z} \equiv \{Z_j = 1, \dots, N_z\}$ of independent variables defining the shape of a stellarator configuration is large. For example, the configuration boundary is often represented by a set of Fourier amplitudes, of which several tens are needed for a typical design. To find attractive design points in this space, or to understand operational flexibility about a given design point, one needs insight into the topography in \mathbf{Z} -space of various physics figures of merit $\mathbf{P} = \{P_i(\mathbf{Z})\}$ ($i = 1, \dots, M_p$) which characterize the machine performance (e.g., transport, kink stability, etc.).

An important new means for stellarator design made possible by advances in physics codes and computational power is the use of automated optimizers. For example, the National Compact Stellarator Experiment (NCSX) design group has made extensive use of an optimizer in developing candidate configurations for an attractive Quasi-Axisymmetric (QA) stellarator (QAS) design.¹ The optimizer conducts a search in a \mathbf{Z} -space describing the stellarator boundary, using an objective function $F(\mathbf{P})$ which is a function of the P_i of the configuration. While a powerful tool, the optimizer is searching a large space whose topography has been essentially unknown, and there is limited understanding of why the optimizer arrives at the design points \mathbf{Z}_0 it does. Deeper insight into this would enhance our ability to locate attractive design points [e.g., by reducing the dimensionality of the \mathbf{Z} -space, or by recognizing topographical features which point to superior “valleys” of $F(\mathbf{P})$ in the \mathbf{Z} -space], and to examine operational flexibility about those points. Such insight can be used both to better focus the operation of an optimizer, as well as to enhance human understanding of the configurations being studied.

The control matrix (CM) approach discussed here helps provide this insight. The approach we discuss has both local and global aspects. As narrowly defined, the CM is simply the matrix $C_{ij} \equiv \partial P_i / \partial Z_j$ of first derivatives at any point \mathbf{Z}_0 in \mathbf{Z} -space, and so can give topographical information only

locally. One may provide more information by expanding to second and higher orders, and most globally, one may investigate the full nonlinear variation over ranges where a power-series expansion is not practical. But even to compute the derivatives needed for C_{ij} correctly, one needs to know the characteristic scales on which the P_i vary in \mathbf{Z} , so more global knowledge is important even for the local problem. And as already indicated, the more global information may also be important in locating genuinely different stellarator optima. Thus, in this paper we address both the more local and more global sides of this topographical exploration.

It should be noted that the technique of “function parametrization” (FP) has been used to provide an approximate global description of the $P_i(\mathbf{Z})$ for tokamak² and stellarator³ equilibria, for fast interpretation of equilibria from experimental data. This useful method is distinct from and sometimes complementary to the CM analysis employed here, as discussed at the end of Sec. II A.

In Sec. II we describe the mathematical basics of the CM method, and discuss the means we use to reduce the dimensionality of \mathbf{Z} -space. Implementing the CM procedure requires exploring the scales of variation of the P_i in \mathbf{Z} in the vicinity of a design point \mathbf{Z}_0 , for which we choose “C10,” a candidate NCSX configuration. This is done in Sec. III. Our topographical study here finds that within an appreciable domain (variations in the Z_j of order 1 cm) about C10, the P_i may be well approximated by simple quadratic expressions, and in addition, we are able to reduce the dimensionality of the \mathbf{Z} -space we need to consider from an initial $N_z = 78$ to 8. As a result, in Sec. IV we apply the machinery of the local CM analysis to a greatly reduced parameter space, and within that space can compute quantities of interest using analytically tractable quadratic expressions for the P_i . We then provide the “proof of principle” of the CM method, demonstrating that the CM mathematics correctly produces perturbations ξ^i with which we can independently vary the P_i , and “nullspace” perturbations \mathbf{v}^i which produce differ-

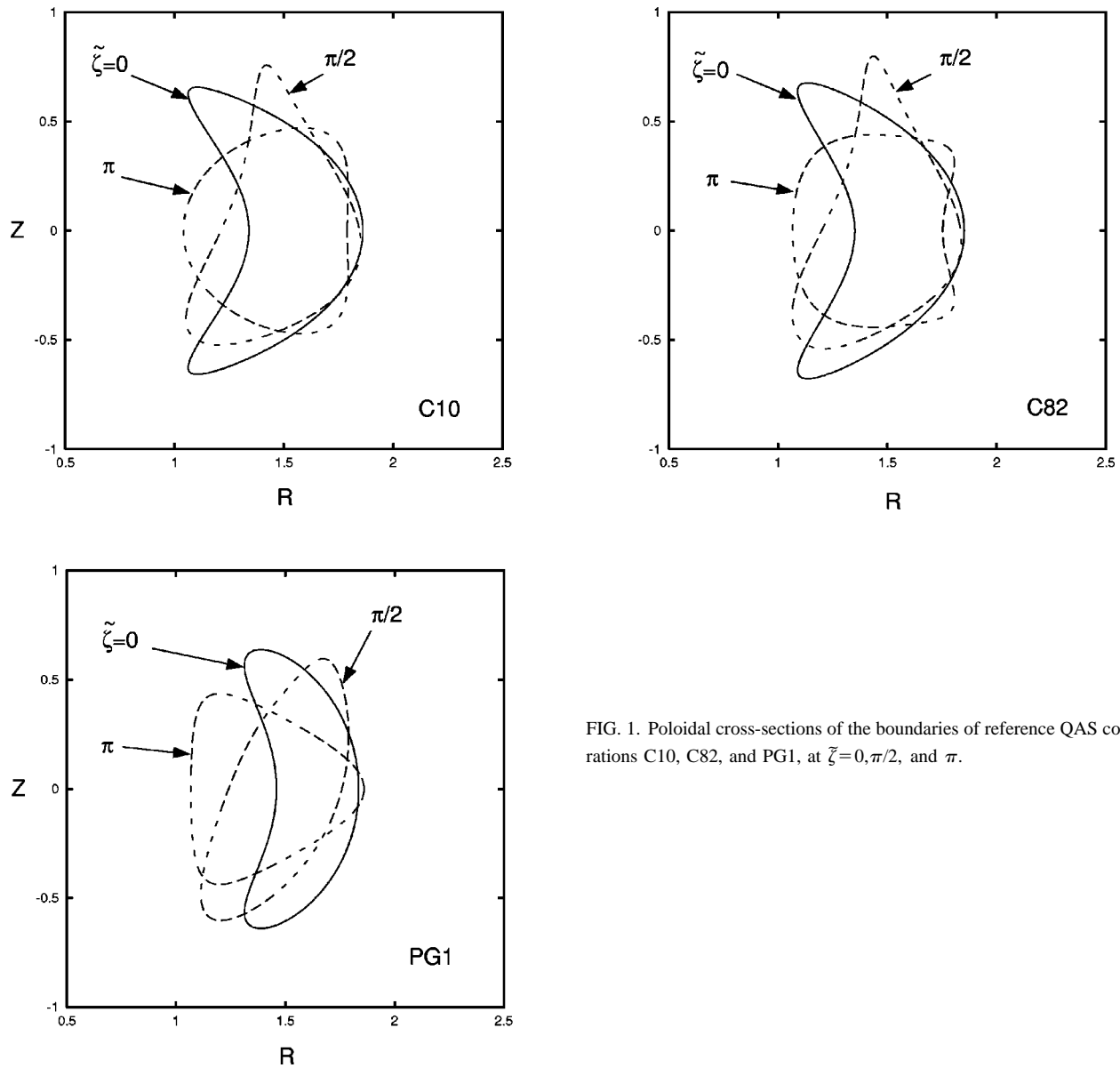


FIG. 1. Poloidal cross-sections of the boundaries of reference QAS configurations C10, C82, and PG1, at $\tilde{\zeta}=0, \pi/2$, and π .

ent configurations, but with unchanged values of the P_i . We discuss some of the features of these perturbations. In Sec. V we move to a more global exploration of \mathbf{Z} -space, applying some of the same machinery used in earlier sections to study the variation of the P_i en route to candidate QAS configurations other than C10. In Sec. VI we summarize the findings of the earlier sections, and discuss applications of the CM approach now in progress or planned for the near future.

II. FORMULATION

A single stellarator configuration may be described by a set of Fourier amplitudes, $\mathbf{X} = \{X_{j=1, \dots, N_x}\} \equiv (R_{n_1}, Z_{n_1}, R_{n_2}, \dots, Z_{n_{N_x/2}})$ which define the plasma boundary $[R(\theta, \zeta), Z(\theta, \zeta)]$. Here, $\mathbf{n} \equiv (\tilde{n} = n/N_p, m)$ are toroidal and poloidal mode numbers per period, with N_p equal to the number of field periods. For C10 and C82, two candidate NCSX configurations⁴ we shall consider in this paper, the

number of Fourier amplitudes is $N_x = 78$ corresponding to maximum mode numbers of $\tilde{n}_{\max} = 3$, and $m_{\max} = 5$. PG1, a third QAS configuration⁵ discussed in Sec. V, has $N_x = 32$. Figure 1 shows poloidal cross sections of the plasma boundary for these three configurations.

Various measures of stellarator transport and stability are used as figures of merit in the cost function of the full configuration optimizer.¹ QA stellarators are an approach to transport optimization based on making the magnetic field amplitude $B(\mathbf{x})$ look axisymmetric in Boozer coordinates, as does that for a tokamak. Thus, the degree to which a design has achieved transport optimization, closely related to its degree of nonaxisymmetry, is an important measure of the performance of such machines. Because of the resemblance to tokamaks, appreciable toroidal current is an intrinsic aspect of such stellarators, and, thus, stability to kink modes has been found to be a major limiting factor on the achievable beta of these configurations, with ballooning stability also playing a significant role, and these figures of merit are ac-

cordingly also important contributors to the optimizer objective function. The evaluation of all figures of merit require the calculation of a magnetohydrodynamic (MHD) equilibrium, performed using the VMEC⁶ code. To evaluate the transport, the magnetic fields output by VMEC in a non-straight coordinate system are re-expressed in terms of the Boozer coordinate system using the JMC code.⁷ The various measures of transport used by the optimizer are then easily expressed in terms of the Fourier components, B_{mn} , of the magnitude of the magnetic field. For stability, both internal ballooning and free-boundary kink modes are evaluated using the TERPSICHORE code.⁸

In this paper, we use the same suite of codes employed by the optimizer, and compute $M \equiv M_p = 5$ figures of merit $\mathbf{P} = (\chi_1^2, \chi_2^2, W_1, W_2, \lambda)$. P_{1-4} are 4 measures of the ripple strength, and hence the level of nonaxisymmetric transport one may expect, and P_5 is a measure of stability. More specifically, $\chi_{1,2}^2 \equiv \chi^2(s_{1,2})$, where $\chi^2(s) = \sum_{m,n \neq 0} B_{mn}^2 / B_{00}^2$ and $s_{1,2}$ label two magnetic surfaces within the plasma volume containing a fixed amount of toroidal flux. The selected values of s (normalized to unity at the plasma edge) are $s_1 = 0.5$, and $s_2 = 0.71$. $W_{1,2} \equiv W(s_{1,2})$ is the ‘‘water function’’⁹ at $s_{1,2}$, measuring the average ripple-well depth along a field line. The fifth figure of merit is $P_5 \equiv \lambda = \omega^2$, the most unstable kink eigenvalue computed by TERPSICHORE (negative for unstable modes). We consider four QA-associated figures of merit for the purposes of comparison among them. A single one may be used for the purposes of configuration analysis, and we shall do so at appropriate points in the paper. Other figures of merit might be usefully added to the present set, such as the ballooning growth rate, surface quality, or coil complexity, and the same formal machinery employed to study any such set.

$N_x = 78$ is a large space to search, and one important objective here is to reduce this number to a more manageable value. That is, we seek a ‘‘reduced space’’ \mathbf{Z} contained in \mathbf{X} , with dimensionality $N \equiv N_z \ll N_x$ which is as small as possible while retaining the most important physics. We discuss means by which this can be done in Sec. II B. We think of \mathbf{Z} as the space of ‘‘control knobs’’ at our disposal, to which the CM machinery is applied, and thus its exact relation to the concrete specification of \mathbf{X} already given may change, depending on the application. For example, in Sec. VI we take \mathbf{Z} to be a set of amplitudes describing the coil currents, for considerations of coil design or operational flexibility. However, for most of this paper, \mathbf{Z} will be a linear subspace of \mathbf{X} , given by amplitudes specifying the plasma boundary.

A. Control matrix basics

In the reduced space, expanding $\mathbf{P}(\mathbf{Z} = \mathbf{Z}_0 + \mathbf{z}) = \mathbf{P}(\mathbf{Z}_0) + \mathbf{p}$ about $\mathbf{Z} = \mathbf{Z}_0$, one has (writing in component-form, with the summation over repeated indices assumed, unless otherwise indicated)

$$p_i(\mathbf{Z}_0 + \mathbf{z}) = C_{ij}(\mathbf{Z}_0)z_j + \frac{1}{2}H_{ijk}(\mathbf{Z}_0)z_jz_k + (\text{h.o.}), \quad (1)$$

with linear coefficients given by the $M \times N$ ‘‘control matrix’’ C_{ij} , quadratic coefficients given by the ‘‘Hessian’’ H_{ijk} ,

and h.o. \equiv higher-order terms. For small enough \mathbf{z} that only linear terms are needed, one has the matrix equation

$$\mathbf{p} = \mathbf{C}_0 \cdot \mathbf{z}, \quad (2)$$

with $\mathbf{C}_0 \equiv \mathbf{C}(\mathbf{Z}_0)$ the control matrix at design point \mathbf{Z}_0 . This may be inverted, using the Singular Value Decomposition (SVD) theorem,¹⁰

$$\mathbf{C}_{M \times N} = \mathbf{U}_{M \times N} \cdot \mathbf{\Sigma}_{N \times N} \cdot \mathbf{V}_{N \times N}^T, \quad (3)$$

with \mathbf{U}, \mathbf{V} unitary matrices, and $\mathbf{\Sigma}$ a diagonal matrix whose diagonal elements σ_i are the ‘‘singular values’’ of the problem. This theorem permits one to obtain a ‘‘pseudo-inverse’’ \mathbf{C}^+ of the nonsquare matrix \mathbf{C} , and provides bases spanning its range and nullspace.

Taking the particular basis set $\boldsymbol{\pi}^i = \mathbf{1}^i$ in the target \mathbf{P} -space to be the set of unit vectors with 1 in the i th position and 0 elsewhere, one has the corresponding set $\boldsymbol{\xi}^i$ of displacements in \mathbf{Z} -space

$$\boldsymbol{\xi}^i \equiv \mathbf{C}_0^+ \cdot \boldsymbol{\pi}^i, \quad (4)$$

where $\mathbf{C}_0 \equiv \mathbf{C}(\mathbf{Z}_0)$. The $\boldsymbol{\xi}^i$ physically represent displacements which change a single physics parameter P_i by unity, leaving the others unchanged. These span the range of \mathbf{C} . The $(N-M)$ vectors $\mathbf{v}^i (i = M+1, \dots, N)$ spanning the nullspace of \mathbf{C} (which change the configuration without modifying any of the P_i) are the orthonormal set formed by those columns of \mathbf{V} with i such that $\sigma_i = 0$. These are also important, permitting one to find different stellarator boundaries which have the same physics performance, giving flexibility for other criteria, e.g., improved coil design. Together, $\boldsymbol{\xi}^{i=1, \dots, M}$ and $\mathbf{v}^{i=M+1, \dots, N}$ span \mathbf{Z} .

For somewhat larger \mathbf{z} , but still small enough that only up to H_{ijk} need be kept in Eq. (1), one can compute the control matrix for any \mathbf{Z} in this region, via

$$C_{ij}(\mathbf{Z}) \equiv \partial p_i(\mathbf{Z}) / \partial z_j = C_{ij}(\mathbf{Z}_0) + H_{ijk}z_k, \quad (5)$$

and from this, find the correct $\boldsymbol{\xi}^i$ at any \mathbf{Z} , along with simple linear expressions for the extrema \mathbf{z}^i of the P_i , etc. We shall find that this ‘‘quadratic model’’ is valid in an appreciable neighborhood about C10, and shall explicitly compute and make use of C_{ij} and H_{ijk} in Sec. III.

The \mathbf{z}^i are easily solved for using Eq. (5). For any i , we may write H_{ijk} in matrix notation as \mathbf{H}_i , which is a square, symmetric, $N \times N$ matrix, invertible by standard means. Then from Eq. (5), one has

$$\mathbf{z}^i = -\mathbf{H}_i^{-1} \cdot \mathbf{c}_0^i, \quad (6)$$

where vector \mathbf{c}_0^i is the i th row of matrix \mathbf{C}_0 , and no summation over i is implied. Similarly, taking our objective function to be a linear combination of the P_i with weights w_i , $F(\mathbf{P}) = w_i P_i$ (summation implied), one can readily solve for the extremum \mathbf{z}^F of $F(\mathbf{P})$:

$$\mathbf{z}^F = -\mathbf{H}_F^{-1} \cdot \mathbf{c}_0^F, \quad (7)$$

with $\mathbf{H}_F \equiv w_i \mathbf{H}_i$ and $\mathbf{c}_0^F \equiv w_i \mathbf{c}_0^i$. Expression (7) thus gives the design point sought by an optimizer. However, as for Eq. (6), for it to be correct, \mathbf{z}^F must fall within the domain of validity of the quadratic model for the $P_i(\mathbf{Z})$. An optimizer using a steepest-descent method would step opposite the direction of

the \mathbf{Z} -space gradient $\partial_{\mathbf{Z}}F \equiv \partial F / \partial Z_j$. For the chosen form for F , this is $\partial F / \partial Z_j = (\partial F / \partial P_i)(\partial P_i / \partial Z_j) = w_i C_{ij} \equiv w_i(\mathbf{c}^i)_j \equiv (\mathbf{c}^F)_j$. Using this with (5) gives

$$\partial_{\mathbf{Z}}F = \mathbf{c}^F = \mathbf{c}_0^F + \mathbf{H}_F \cdot \mathbf{z}. \quad (8)$$

From this and Eq. (7), one sees that at $\mathbf{z} = \mathbf{z}^F$ one has $\partial_{\mathbf{Z}}F = 0$, as one expects. Additionally, using Eqs. (4) and (8), one finds that the component of ξ^i in the direction of this gradient is $\partial_{\mathbf{Z}}F \cdot \xi^i = w_i$.

The $P_i(\mathbf{Z})$ provide M coordinates of a special global coordinate system on \mathbf{Z} -space, chosen to characterize the physics performance of the stellarator. One may imagine supplementing these by a further set $\{Q_i(\mathbf{Z})\}$, ($i = M + 1, \dots, N$) of functionally independent quantities to fully parametrize \mathbf{Z} , also chosen on the basis of their physical relevance or independence from stellarator performance. Obtaining the (nonlinear) transformation between the control knobs Z_j and the performance parameters P_i and Q_i lies at the core of the stellarator design. At each point \mathbf{Z} , the basis set $\{\xi^i, i = 1, \dots, M, \mathbf{v}^i, i = M + 1, \dots, N\}$ coming from the CM formulas introduced here provides a local description of this performance-based coordinate system, with the ξ^i performing a role akin to that of the reciprocal basis vectors \mathbf{e}_i of the contravariant representation $A^i \mathbf{e}_i$ of any vector \mathbf{A} , pointing in a direction normal to the gradients of all P_i but that with the specified i .

As noted in Sec. I, the FP method,^{2,3} which also is applied to describe the P_i over \mathbf{Z} -space, is a technique serving a different purpose from the local CM analysis employed here, which may sometimes be used in conjunction with it. The method provides an approximate global description of the $P_i(\mathbf{Z})$ (the starting point for the CM method), by taking a randomly distributed ensemble of equilibria in \mathbf{Z} -space, and fitting the $P_i(\mathbf{Z})$ of these by some simple functional model, e.g., a polynomial in the Z_j . Thus, if desired, the local CM analysis could be applied to the $P_i(\mathbf{Z})$ provided by FP, which would then yield the ξ^i and \mathbf{v}^i for the approximate FP topography in the vicinity of some reference point \mathbf{Z}_0 . However, unless the approximate description is quite accurate *locally*, the directions of these CM vectors will be very different from those for the exact $P_i(\mathbf{Z})$, and therefore of uncertain utility. Obtaining adequate accuracy with the FP method requires a much larger ensemble of equilibria than with the local method used here to compute C_{ij} , if the domain about \mathbf{Z}_0 is large enough that the simpler method used here is inadequate. The strength of the FP approach is not local accuracy, but representing the $P_i(\mathbf{Z})$ correctly *in the large*, while the local CM method requires the correct $P_i(\mathbf{Z})$ *locally*. On the other hand, regarding global analysis, the results presented here are only a preliminary exploration of \mathbf{Z} -space. Here, the FP analysis may provide a good means for a more detailed future study.

B. Reducing the dimensionality of \mathbf{Z}

The CM framework just described may be applied to the full $N_x = 78$ dimension space \mathbf{X} , or to any subspace \mathbf{Z} of that space. Before applying the method in the vicinity of configu-

ration C10, it is useful to begin reducing the dimensionality N_z of \mathbf{Z} . In this paper, we shall use two methods to accomplish reductions.

- First, as pointed out by Hirshman and Breslau,¹¹ there is a redundancy in the \mathbf{X} -specification, with many perturbations \mathbf{x} of \mathbf{X} modifying the *representation* of the boundary, rather than the boundary shape itself. The equivalent nonredundant representation we present in this section produces a reduction of a factor of 2, yielding a nonredundant subspace $\mathbf{Y} \subset \mathbf{X}$ of dimension $N_y = 39$ for the C10–C82 family.
- In Sec. III, we further reduce N_z from 39 to 8, by selecting only the perturbations most effective in varying the P_i of interest, resulting in an approximate “reduced-model” description of configuration space.

Regarding reduction (a), independent variations in R_{mn} and Z_{mn} produce not just changes in the physical shape of the plasma boundary, but also changes in the poloidal angle variable, which is not uniquely defined. A nonredundant boundary deformation is made by instead prescribing the linear combinations of the R_{mn}, Z_{mn} that define *normal* displacements (at each ϕ plane) to the plasma boundary. For a plasma boundary in real space \vec{X} defined by

$$\vec{X}(\theta, \phi) = R(\theta, \phi)\hat{R}(\phi) + Z(\theta, \phi)\hat{Z}, \quad (9)$$

a general displacement is $\vec{Y} = \delta\vec{X} = \delta R\hat{R} + \delta Z\hat{Z}$, and a normal displacement is¹³

$$\vec{Y} \cdot \frac{\partial \vec{X}}{\partial \theta} \theta \times \frac{\partial \vec{X}}{\partial \phi} \phi = R \left(\frac{\partial R}{\partial \theta} \delta Z - \frac{\partial Z}{\partial \theta} \delta R \right). \quad (10)$$

Multiplying by $\cos(m\theta + n\phi)$ and integrating over θ and ϕ yields a matrix equation in the form

$$Y_i = \sum_j B_{ij} X_j. \quad (11)$$

Here, as earlier, $\mathbf{X} \equiv \{X_j, j = 1, \dots, N_x\}$ is the set of Fourier expansion coefficients of both δR and δZ , while $\mathbf{Y} \equiv \{Y_i, i = 1, \dots, N_y\}$ is the set of Fourier coefficients of the normal displacement to the plasma boundary, and B_{ij} is the $N_y \times N_x$ rectangular influence matrix that relates the two. To compute the X_j required by VMEC in terms of the Y_i , we employ the same SVD decomposition as in Eq. (3) to invert the matrix B_{ij} .

Before we can apply the approximate reduction method (b) or take the numerical derivatives needed to carry out the CM prescription, we need to ascertain the scales of variation of the P_i in the \mathbf{X} - or \mathbf{Y} -space. This is done in the following section.

III. TOPOGRAPHY OF \mathbf{Z} -SPACE NEAR C10

The validity of Eqs. (1) or (2) depends on the typical scales of variation in \mathbf{Z} -space of the P_i , which previously have been largely unknown. In the vicinity of the C10 family of configurations, we have assessed this variation for the P_i presently being used for all 78 X_j as well as for the nonredundant amplitudes Y_j .

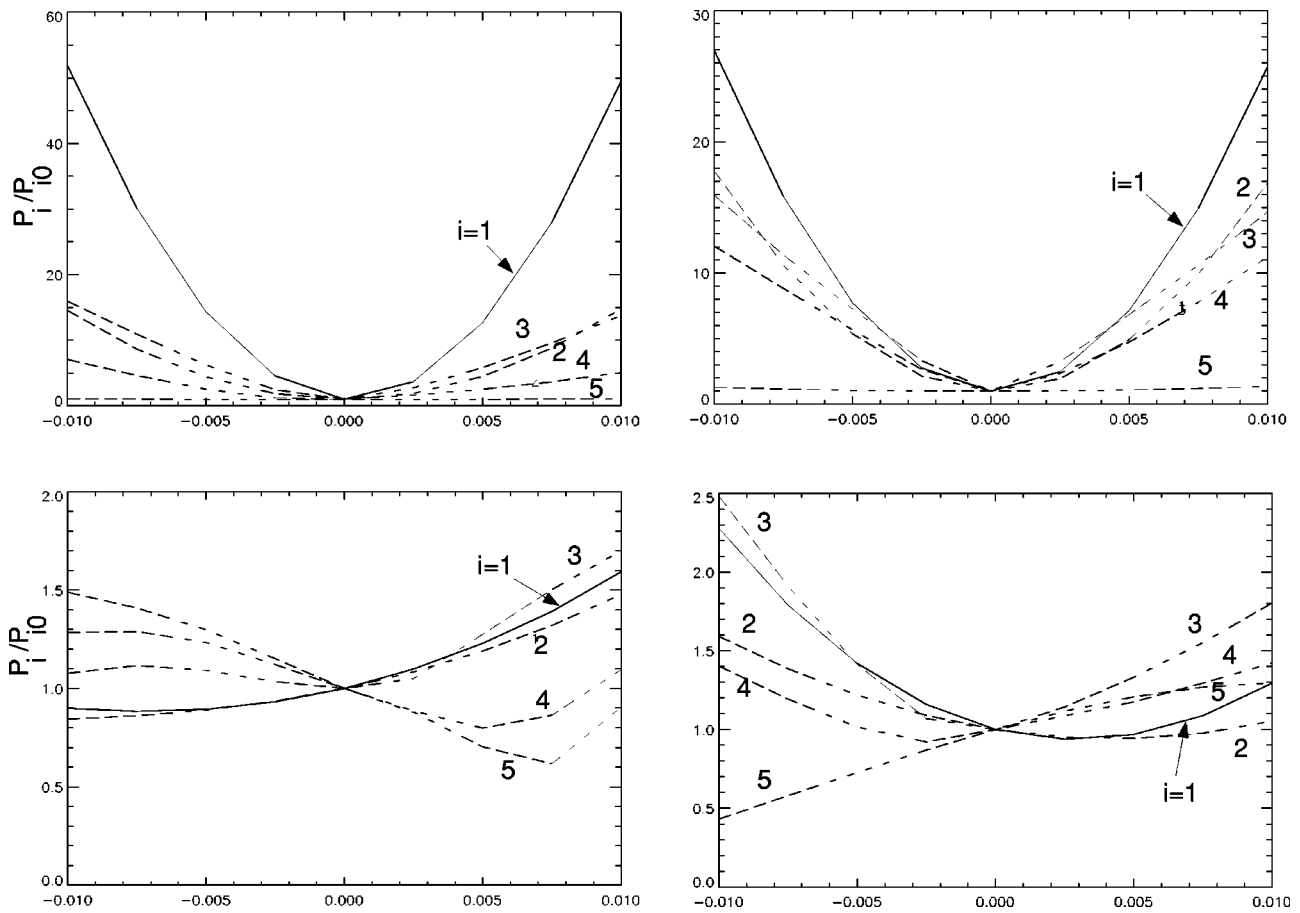


FIG. 2. Variation of figures of merit $P_{i=1-5}$ computed from VMEC and TERPSICHORE, of equilibria with deformation amplitude z_j (in meters), for representative harmonics $\mathbf{n}_j = \{(1,0), (-3,1)\}$ (top) and $\{(1,3), (2,4)\}$ (bottom). See Sec. II, paragraph 3 for definitions of the P_i .

Some typical results in the space $\mathbf{Z} = \mathbf{Y}$ are shown in Fig. 2, showing the variation of the P_i computed from VMEC and TERPSICHORE with deformation amplitude $z_j \equiv \delta Z_j$ (in meters) of the given $Z_j = Y_j$. Four harmonics \mathbf{n}_j are shown. The top two are for $\mathbf{n} = \{(1,0), (-3,1)\}$, to which the QA measure P_1 is sensitive, and the bottom two are for $\mathbf{n} = \{(1,3), (2,4)\}$, to which the kink eigenvalue P_5 is rela-

tively sensitive. The size of the domain shown ($\Delta Z_j = \pm 0.01$ m) is appreciable, large enough to encompass C82 as well as C10 (see Sec. V A).

Probably because of the symmetrizing action of the optimizer in creating C10, most directions Z_j resemble the top pair: the fractional variation P/P_0 of $P_1(Z_j)$ is much larger than that for P_5 (reflecting the near-optimal value of the

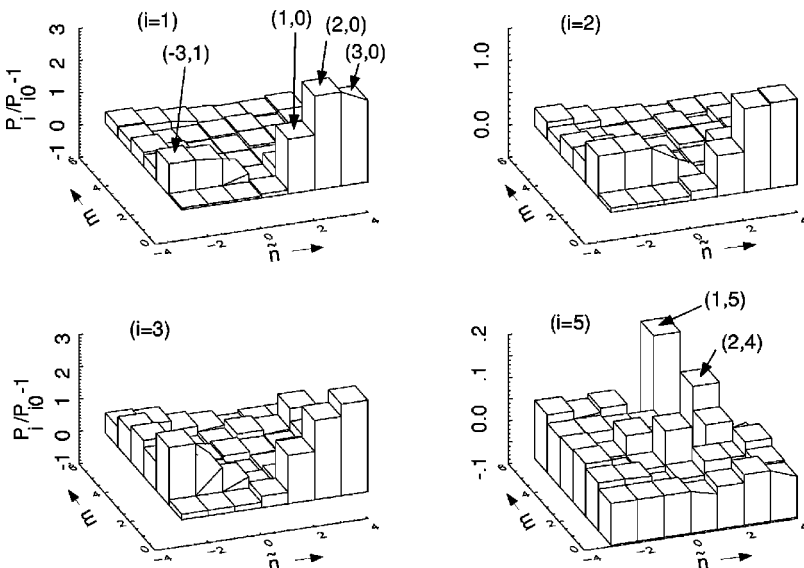


FIG. 3. Histograms of the fractional variation $P_i/P_{i0} - 1$ for $i=1-3$ and 5 over the full (\tilde{n}, m) -plane for C10, for a fixed variation $dZ=0.002$ m in amplitudes Z_j .

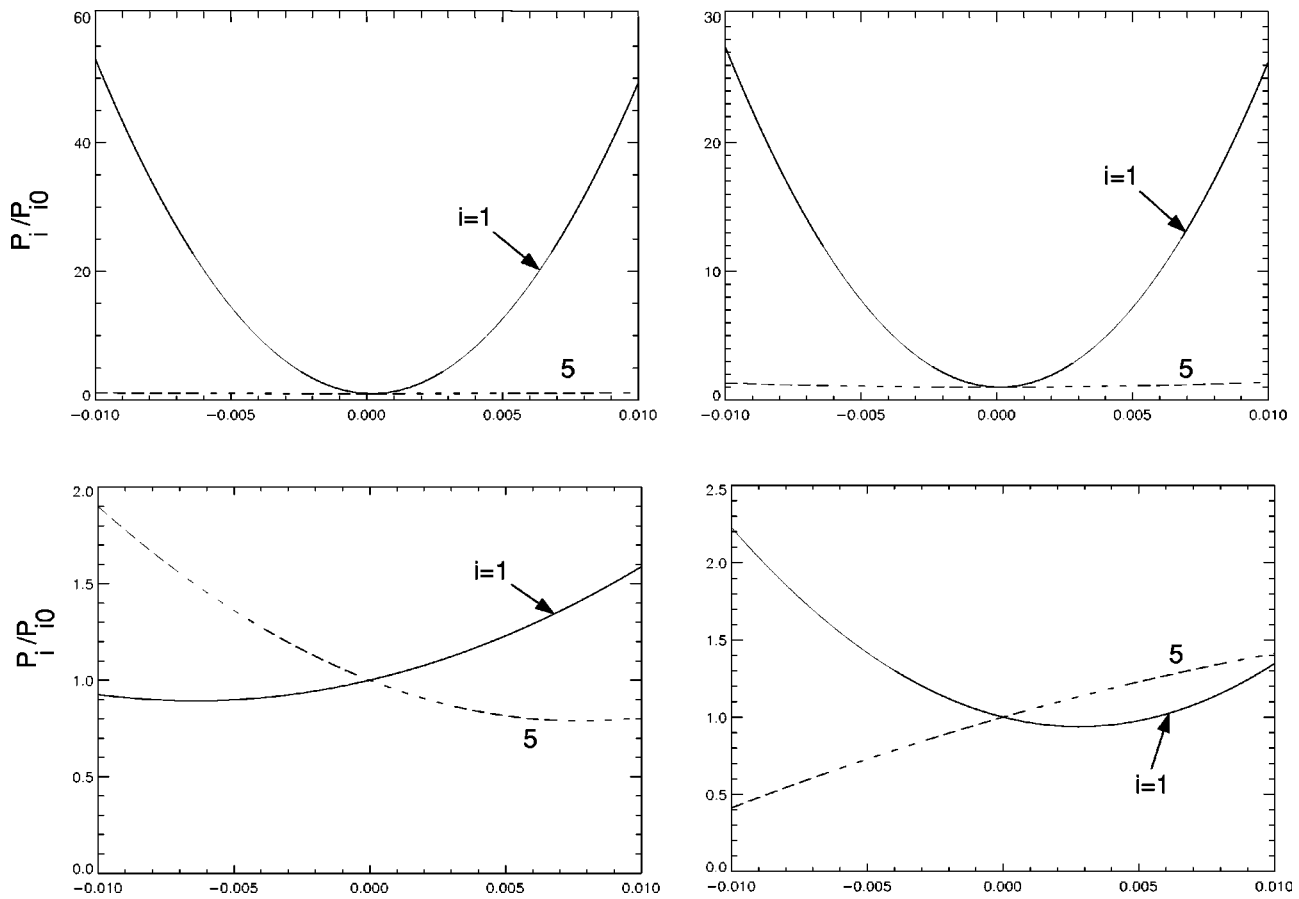


FIG. 4. Variation of $P_1 = \chi_1^2$ and $P_5 = \lambda$ with deformation amplitude z_j for the same harmonics as in Fig. 2, but computed from the quadratic approximation of Eq. (1).

unperturbed P_{10} in the denominator), and P_1 is a parabolic curve, with vertex often near $z_j=0$. For all Z_j , the variation of both P_i is smooth and rather unstructured, approximable by the quadratic expansion (1) over all or most of this domain.

Given this knowledge, in Fig. 3 are shown histograms of the fractional sensitivity $(P_i/P_{i0} - 1)$ over the (\tilde{n}, m) -plane (hence showing all Z_j), for $i=1-3$ and 5, and for a fixed value $dZ=0.002$ m for each z_j , a modest fraction of the Z_j scale length just shown in the plots of Fig. 2. (The $i=4$ histogram is not shown simply to conserve space.) Though the QA measures $P_{i=1-4}$ are linearly independent, their histograms are quite similar, and these are markedly different from that for the kink measure P_5 .

With the information in the sensitivity histograms, we can apply reduction method (b) introduced in Sec. II. We rank the harmonics, selecting the 4 to which P_1 is most sensitive, and the 4 to which P_5 is most sensitive, resulting in a final reduced model with $N_z=8$ harmonics. We have chosen a single one of the 4 QA-associated P_i as representative of QA measures, confirmed from the similarity of the curves for $P_{i=1-4}$ in Fig. 2. The choice of four harmonics for each is somewhat arbitrary, chosen to produce a relatively simple system on which to develop the CM machinery, yet rich enough to display the control flexibility we are

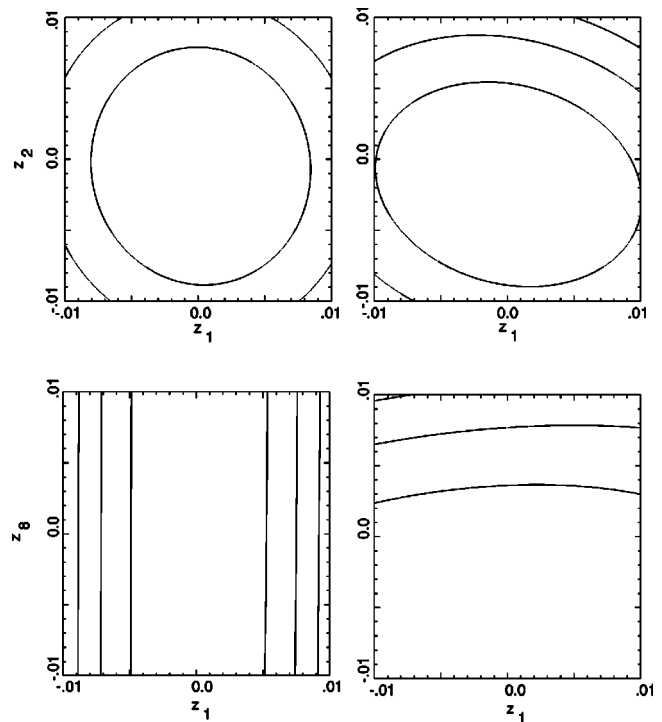


FIG. 5. Contour plots of P_1 (left) and P_5 (right) over the (z_1, z_2) plane (top) and (z_1, z_8) plane (bottom).

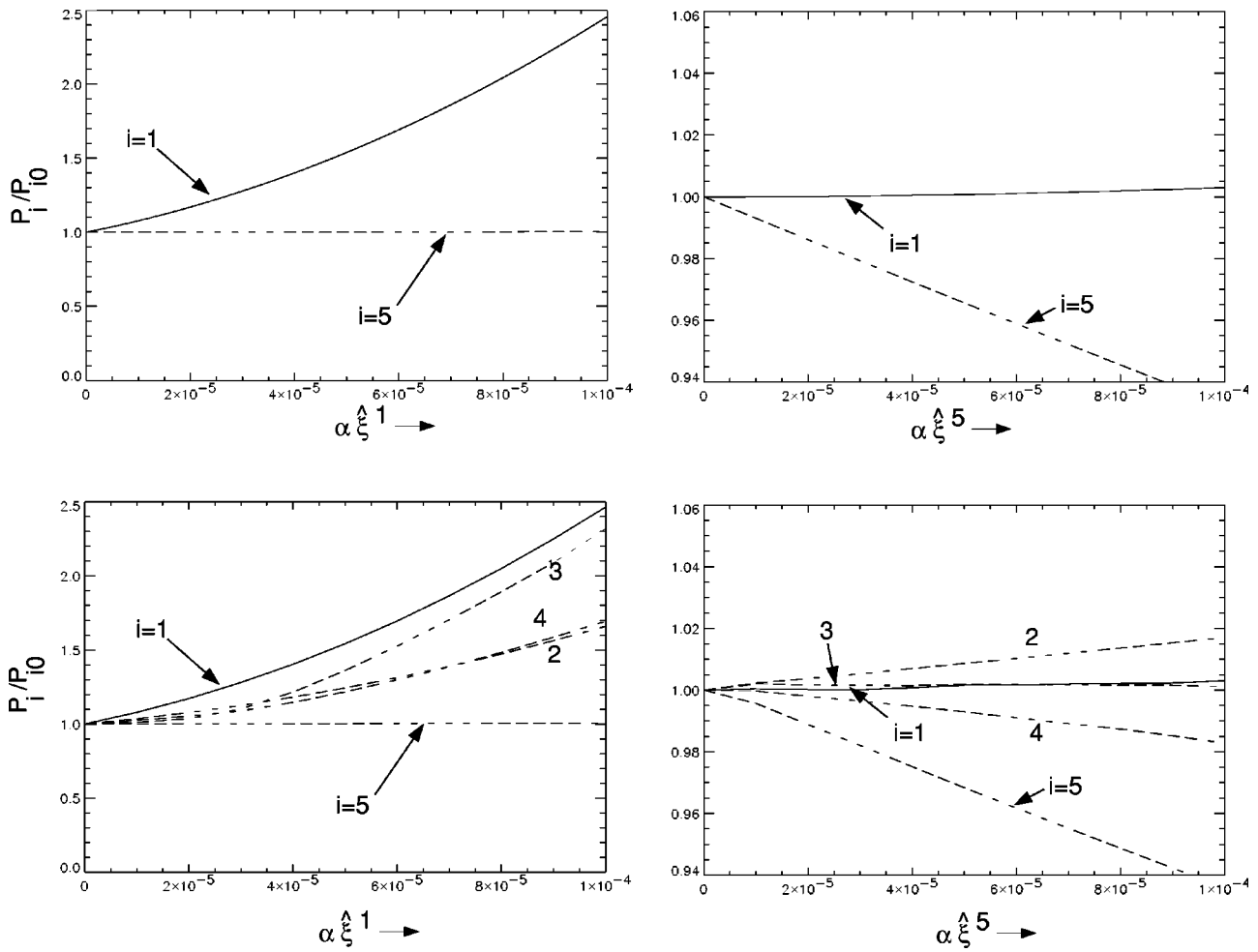


FIG. 6. A comparison of the analytical (top row) versus numerical (bottom row) variation of $P_{1,5}$ for perturbations $\alpha \xi^1$ (left) and $\alpha \xi^5$ (right), confirming that these displacements provide independent control over P_1 and P_5 .

seeking. We have examined two $N_z=8$ reduced models, whose difference comes from somewhat different ranking criteria. The models were found to possess similar properties. The criterion for the model presented here is simply taking the harmonics with the largest values of $|P_i/P_{i0} - 1|$. The eight harmonics of this model are accordingly $\mathbf{n}_j = \{(1,0), (2,0), (3,0), (-3,1); (1,3), (1,4), (2,4), (1,5)\}$, with the first four most affecting P_1 , and the last four most affecting P_5 . One notes that the P_1 set (affecting QA-ness) have small m and a range of \tilde{n} , while the P_5 set have $\tilde{n} \sim 1$ or 2 and a range of m . The top two plots of Fig. 2 are seen to belong to the P_1 set, and the bottom two to the P_5 set.

IV. CM ANALYSIS OF THE REDUCED MODEL

Having now established the scales of variation in \mathbf{Y} -space, and selected from sensitivity histograms the Y_j comprising our reduced model, we are in a position to evaluate the CM tensors C_{ij} and H_{ijk} and from these the vectors \mathbf{z}^i , ξ^i , and \mathbf{v}^i introduced in Sec. II, and to demonstrate that these have the intended properties described in that section. In addition to the base configuration \mathbf{Z}_0 , which we take to be C10, $2N_z^2$ perturbed points \mathbf{Z} must be evaluated for computing the H_{ijk} , including $2N_z$ points also needed for the C_{ij} .

For $N_z=8$, this gives $2N_z^2=128$ points to which VMEC, JMC, and TERPSICHORE must be applied, an appreciable but manageable computational task.

A. Quadratic model

Performing the evaluation of C_{ij} and H_{ijk} , in Fig. 4 we provide a first check that the resultant quadratic model of the $P_i(\mathbf{Z})$ is behaving as it should, plotting P_1 and P_5 versus the same 4 Z_j as shown in the numerical results of Fig. 2. One notes the good agreement. The increment for the required first and second derivatives was $dZ=0.002$ m, which predicts well the values of the P_i for displacements over the range $\Delta Z=0.02$ m shown in Fig. 2 or Fig. 4. Even for $\mathbf{n}=(1,3)$, where P_5 in Fig. 2 cannot be approximated by a quadratic over the full z_j range shown, the quadratic model does well over about the half of the full range near C10 ($z_j=0$).

Using C_{ij} and H_{ijk} , one readily computes the \mathbf{z}^i from Eq. (6). One finds, for example, $\mathbf{z}^1 = \{0.15, -0.38, -0.20, -0.14, -2.11, -14.5, 2.29, 7.66\} \times 10^{-3}$, and $\mathbf{z}^5 = \{-5.35, 1.61, 0.19, 0.26, 0.33, -3.39, 4.97, -4.48\} \times 10^{-3}$ (meters).

In Fig. 5 we visualize the topography in the vicinity of C10, with contour plots of P_1 (left) and P_5 (right) from the

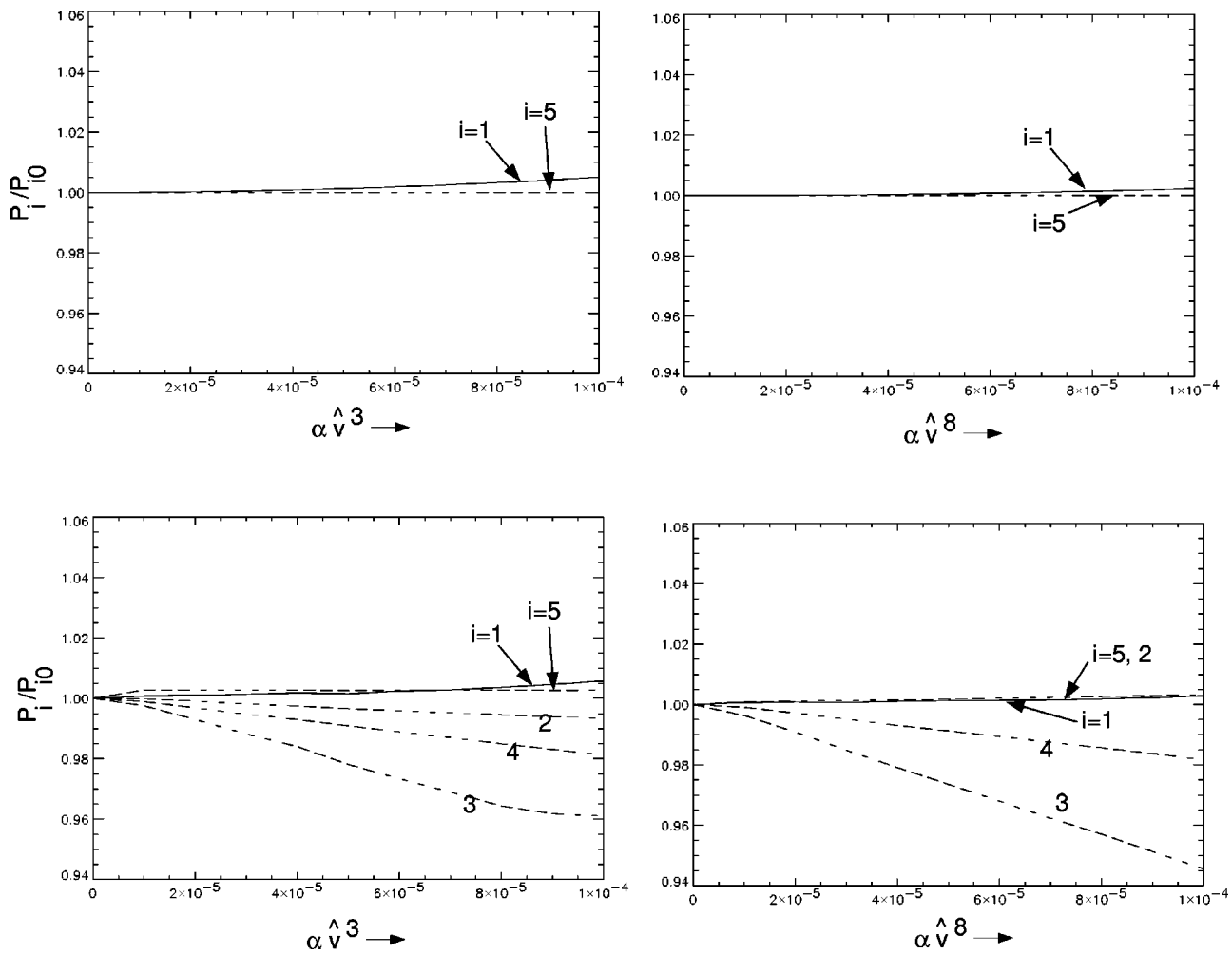


FIG. 7. A comparison of the analytical (top row) versus numerical (bottom row) variation of $P_{1,5}$ for perturbations αv^3 (left) and αv^8 (right), confirming that these nullspace displacements have no effect on P_1 or P_5 .

quadratic model over a plane of two chosen z_j . The top plots are for two QA-related z_j , and the contours for these are elliptical. The bottom plots are for one QA-related and one kink-related z_j , and one notes here that P_1 is almost independent of z_8 , while P_5 is almost independent of z_1 . It is somewhat fortuitous that this property is nearly obeyed for individual z_j ; it need be exactly obeyed only for variations in the ξ^1 and ξ^5 directions.

Applying the SVD-algorithm to invert C_{ij} , we use Eq. (4) to compute the ξ^i and \mathbf{V} from Eq. (3) in obtaining \mathbf{v}^i . As opposed to the \mathbf{z}^i , the values of these depend on how many of the P_i one chooses to keep in C_{ij} . One may keep only P_1 and P_5 , yielding an $M_p=2$ problem with a nullspace of $N_z - M_p = 8 - 2 = 6 \mathbf{v}^i$'s, or solve the more-constrained problem increasing M_p (up to 5, here). Here, we consider the $M_p=2$ problem, obtaining $\xi^1 = \{-3.92, 9.82, 5.99, -1.19, 0.29, 0.55, -0.56, 0.22\}$, and $\xi^5 = \{0.09, -0.78, 0.03, -0.11, 2.77, 2.05, -2.53, -4.10\}$. One notes that the first four components of ξ^1 (the QA-related z_j) are dominant, while the last four components dominate in ξ^5 . While this might be expected, it is not necessary: an independence of (for example) P_1 from ξ^5 could arise from a

cancellation of the effects of appreciable components in ξ^5 of the QA-related z_j .

B. “Proof of principle” of the CM method

Having obtained the ξ^i and \mathbf{v}^i , we can now test the crucial properties discussed in Sec. II of these directions in \mathbf{Z} -space, viz., showing that the boundary perturbations the ξ^i describe actually permit independent control of the P_i , and that those of the \mathbf{v}^i actually leave the P_i unchanged. In this section we provide this key demonstration, and examine some of the features of the deformations these vectors produce.

The demonstration needed is agreement between the analytically-expected variation of the P_i obtained from the quadratic model in the direction of a ξ^i or \mathbf{v}^i , and the variation numerically-obtained from a sequence of equilibria perturbed from C10 in that direction. This comparison is provided in Fig. 6 for perturbations $\alpha \xi^1$ (left) and $\alpha \xi^5$ (right), and in Fig. 7 for perturbations αv^3 (left) and αv^8 (right). Here, α is a scaling parameter, with a value specified on the horizontal axis. The analytic expectations are on the top row,

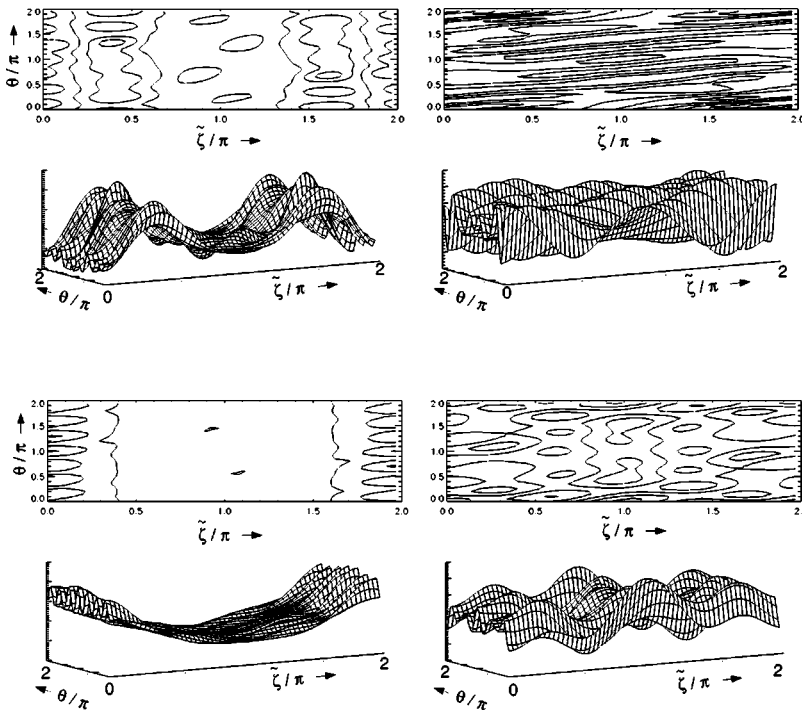


FIG. 8. Contour and surface plots over the $(\theta, \tilde{\zeta})$ -plane of perpendicular displacements ξ_{\perp}^1 and ξ_{\perp}^5 (top), and v_{\perp}^3 and v_{\perp}^8 (bottom).

and the numerical results on the bottom row. One notes that the variations are as expected. Perturbations in the ξ^1 direction do in fact vary P_1 while leaving P_5 unchanged, and similarly for ξ^5 . For the ξ^5 perturbation, there is somewhat more wobble visible in the P_1 curve than for the P_5 curve for the ξ^1 perturbation, because of the greater sensitivity of P_1 to most z_j . Keeping P_1 constant therefore requires a more delicate balance of the harmonics contributing in ξ^5 .

We visualize these perturbations in Figs. 8 and 9. Figure 8 shows contour and surface plots over the $(\theta, \tilde{\zeta})$ -plane of perpendicular displacements ξ_{\perp}^1 and ξ_{\perp}^5 (top), and v_{\perp}^3 and v_{\perp}^8 (bottom). ξ_{\perp}^5 is seen to vary more rapidly with θ and less rapidly with $\tilde{\zeta}$ than ξ_{\perp}^1 , consistent with the harmonic contributions in the sensitivity histograms in Fig. 3. The effect of these perturbations on the boundary are shown in the poloidal cross-section in Fig. 9. In particular, one notes that ξ^5 for diminishing the kink produces an indentation of the outboard side at the half-period $\tilde{\zeta} = \pi$, enhancing the (negative) triangularity which that cross-section possesses. This is consistent with the earlier empirical observation¹ that kink stability can be helped by providing such an indentation. Here, this finding emerges simply from the CM calculation for ξ^5 . However, one also notes that indentation at $\tilde{\zeta} = \pi$ alone is not enough to stabilize the kink: v_{\perp}^8 also causes an indentation. However, its variation with $\tilde{\zeta}$ is markedly different from that of ξ_{\perp}^5 , having an $\tilde{n} = 1$ character, in contrast to the $\tilde{n} = 0$ character for ξ_{\perp}^5 .

V. GLOBAL TOPOGRAPHY: OTHER QAS DESIGN POINTS

C10 and C82 (see Fig. 1) were arrived at along an involved path of human interaction with the optimizer, and it is unclear that other regions of \mathbf{Z} -space, which would have

been reached from different starting points, might not yield superior configurations. Thus, in this section we initiate an exploration of regions of \mathbf{Z} -space farther from C10. As guideposts to promising regions to explore, one can look near other proposed QAS configurations^{5,12} with the same methods. Here, we consider the variation of the P_i as one moves from one such reference point \mathbf{Z}_0 to another.

A. The path from C10 to C82

We begin by considering the P_i along a straight-line trajectory $\mathbf{Z} = \mathbf{Z}_{C10} + \alpha(\mathbf{Z}_{C82} - \mathbf{Z}_{C10})$ connecting C10 with C82, as α runs from 0 to 1. These two configurations are fairly close in \mathbf{Z} -space. We may quantify this by introducing the simple norm: $|\mathbf{X}| \equiv (\sum_j X_j^2)^{1/2}$. With this definition, $|\mathbf{X}_{C82} - \mathbf{X}_{C10}| \approx 0.041$ m, in comparison with the much larger “distance” to PG1 (see below), $|\mathbf{X}_{PG1} - \mathbf{X}_{C10}| \approx 0.228$ m

C82 was obtained from C10 in an effort to stabilize the kink. The level of QA-ness was slightly degraded in compensation. This is borne out by the P_i 's along the straight-line path in \mathbf{Z} -space, shown in Fig. 10. While the kink growth rate falls off to an acceptably low value ($\lambda_{C82}/\lambda_{C10} \approx 0.05$), P_1 actually moves to a somewhat lower value (better quasisymmetry) about midway along the trajectory, and then rises at C82 to a value slightly larger than for C10. One notes that the quadratic approximation would be adequate to describe the variation of the P_i along this trajectory.

B. The path from C10 to PG1

Configuration PG1 (see Fig. 1) is characterized by⁵ much better kink stability ($\lambda > 0$) than C10 or C82, but substantially worse quasisymmetry, due mainly to a large mirror field $B_{m=0, \tilde{n}=1}$ present to assure ballooning stability. As indicated above, its separation from C10 in \mathbf{Z} -space is far

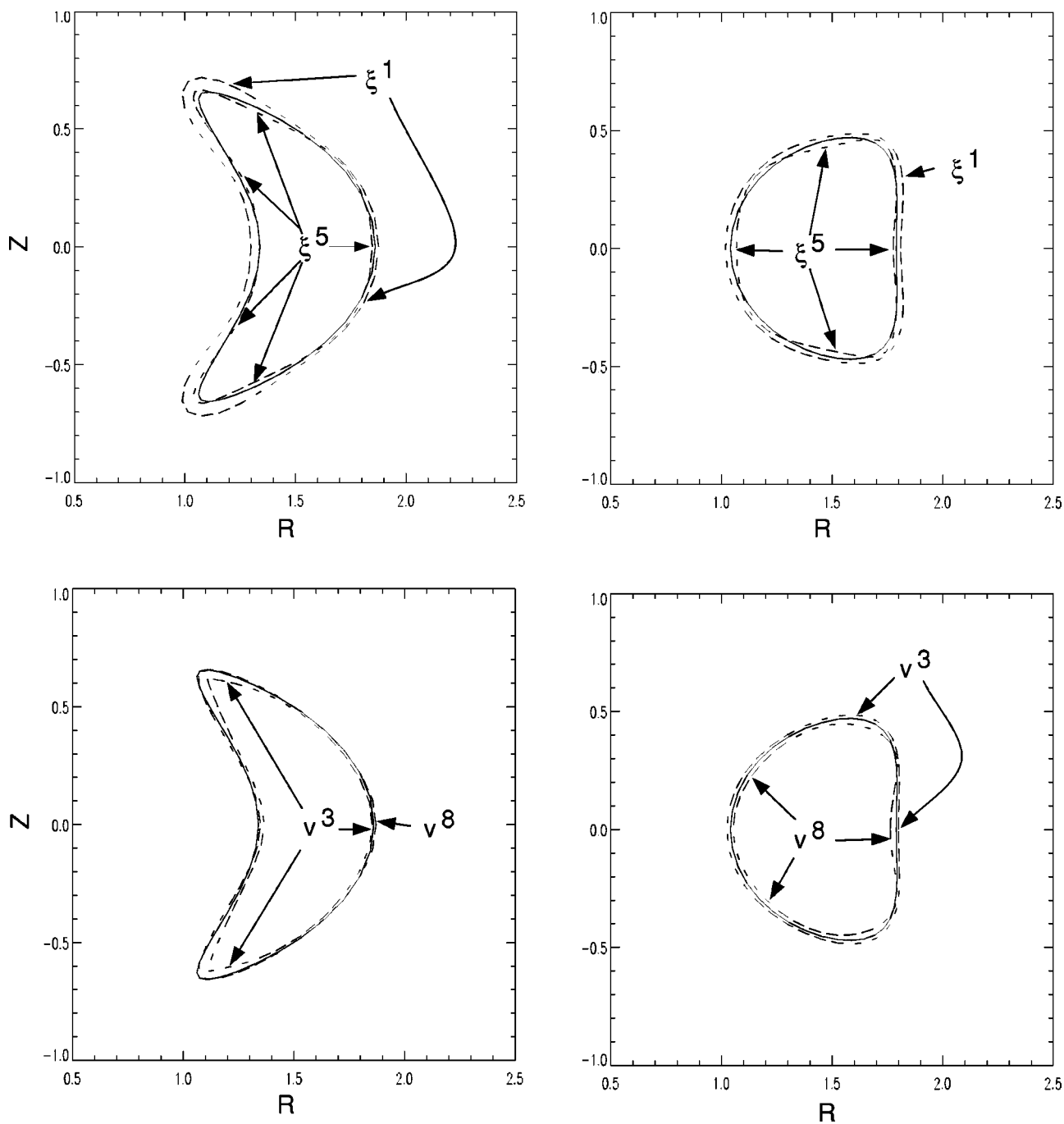


FIG. 9. Poloidal cross-sections of boundaries of C10 (solid curve) and C10 perturbed by $0.002\xi^{1,5}$ and $0.01\nu^{3,8}$ at toroidal positions $\zeta = 0$, and π .

greater than that of C82, and is generally considered to be in a quite different region of Z . Nevertheless, as one sees in Figs. 11, even over this relatively large distance the P_i do not fluctuate greatly, but instead vary smoothly, and almost monotonically, in a manner consistent with the qualitative description of the physics differences given just above between the two stellarators.

Applying the same tools to PG1 as described above for C10, one finds sensitivity histograms for the ξ^i which resemble those for C10. Again, those for $i=1-4$ are similar to each other (and to those for C10), and differ from that for $i=5$. ξ^5 , which reduces the kink growth rate, is found to

enhance the *positive* triangularity which PG1 possesses in the half-period $\zeta = \pi$, consistent with tokamak-based intuition on kink stabilization, an effect opposite that found for C10, which as noted earlier has negative triangularity at $\zeta = \pi$.

VI. DISCUSSION AND SUMMARY

In the foregoing sections we have described and applied the CM approach, mostly in the vicinity of the C10-C82 family of stellarators to which an optimizer has led the NCSX group. For the first time, we are getting a picture of

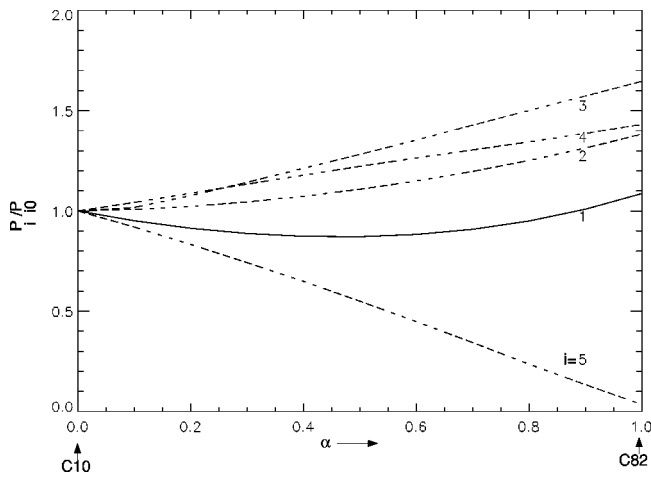


FIG. 10. Plot of the fractional variation P_i/P_{i0} for $i=1-5$ along a straight-line path in \mathbf{Z} -space from C10 ($\alpha=0$) to C82 ($\alpha=1$). These have an \mathbf{X} -space distance between them of 0.041 m.

the topography of the configuration space \mathbf{Z} in which the NCSX optimizer has been searching for good QA stellarators. The local CM method would be applicable and useful even in a \mathbf{Z} -space where the P_i were highly involuted, but instead we find that these are rather smooth and unstructured, even over distances in \mathbf{Z} generally considered large. In an appreciable neighborhood of C10 ($\Delta Z_j \sim 1$ cm) the P_i may be modeled by a quadratic function of $\mathbf{z} = \mathbf{Z} - \mathbf{Z}_0$.

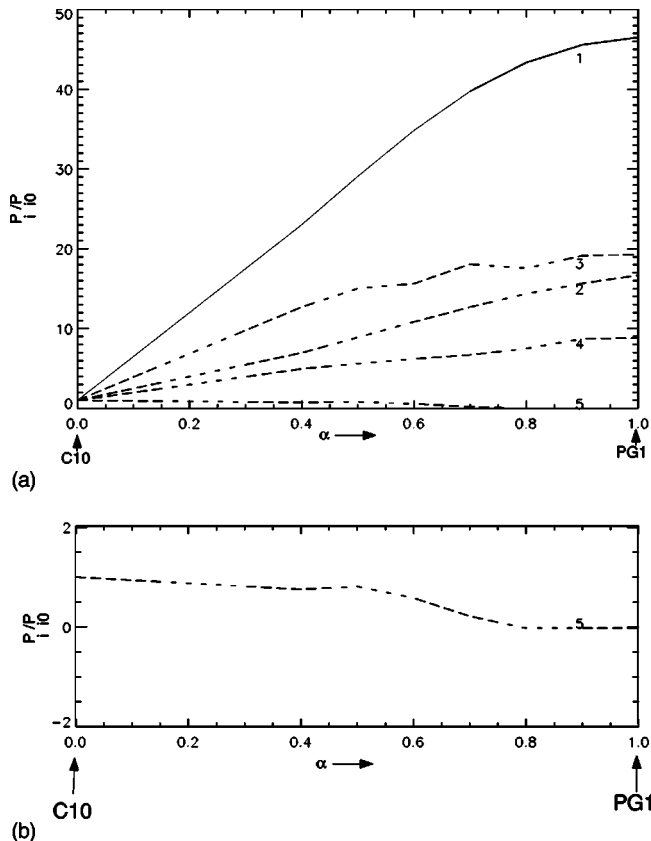


FIG. 11. (a) Plot of the fractional variation P_i/P_{i0} for $i=1-5$ along a straight-line path in \mathbf{Z} -space from C10 ($\alpha=0$) to PG1 ($\alpha=1$). These have an \mathbf{X} -space distance between them of 0.228 m. (b) The same as (a), but with blowup of vertical scale, to show more clearly the variation in P_5 .

From this topographical information, we have produced a restricted configuration space which reduces the dimensionality from $N_z=78$ to 8 while retaining much of the interesting physics in the vicinity of C10, and within this space obtained the first- and second-order coefficients C_{ij} and H_{ijk} describing the simple quadratic variation of the P_i . This permits one to compute quantities of interest for the CM formalism using analytically tractable expressions. We have demonstrated that the CM method produces perturbations ξ^i in \mathbf{Z} with which one can independently vary the P_i , and perturbations \mathbf{v}^i producing different configurations with unchanged values of P_i .

For both C10 and PG1, the sensitivity histograms for $i=1-4$ resemble one another, and differ from that for $i=5$. Correspondingly, the ξ^i for the four different QA-associated figures of merit ($i=1-4$) are similar in appearance, and these differ from that for the kink ($i=5$).

For C10, ξ^5 manifests the outward indentation previously empirically observed to stabilize the kink, enhancing C10's negative triangularity at $N_p \zeta = \pi$, while for PG1, ξ^5 enhances its positive triangularity, consistent with tokamak intuition on kink stabilization.

The work discussed in this study has taken as its free "control knobs" Z_j displacements of the plasma boundary. However, exactly the same procedures may be used to study how a given set of coil currents described by amplitudes $\mathbf{I} \equiv \{I_j\}$ could produce a range of physics behavior \mathbf{P} , with the specialization $Z_j \rightarrow I_j$. Here, the I_j may represent either K_{n_j} , the Fourier amplitudes of the current potential $K(\theta, \zeta)$, for coil design, or J_j , the amount of current in the j th coil of a given coil set, to study operational flexibility. Then the $P_i(\mathbf{Z})$ can be computed almost as done in the present study, but using free-boundary instead of fixed-boundary VMEC.

It will also sometimes be useful to extend the P_i and Z_j beyond the sets specified thus far. For example, to study startup scenarios, the $Z_j=J_j$ could be supplemented to also include $Z_\beta = \langle \beta \rangle$, and perhaps a parameter characterizing the peakedness of the pressure profile. Then, for example, the relative size of Z_β to the other Z_j in the \mathbf{v}^i would specify how the coil currents should be raised as $\langle \beta \rangle$ is during startup in order not to change the QA-ness or kink stability of the machine. For coil design, the P_i could be supplemented to include a measure of coil complexity, e.g., one already used by the NCSX group,^{13,14} $P_6 \equiv \sum_n m^{p+1} K_n^2 / \sum_n m^p K_n^2$, with $p=1-4$. Then applying the CM method just as in the present study, ξ^6 would describe perturbations which would reduce the coil complexity, while maintaining the same physics performance. These and other such applications are planned for future work.

ACKNOWLEDGMENTS

We would like to thank Allen Boozer and Long-Poe Ku for useful discussions, and Steve Hirshman and Tony Cooper for use of VMEC and TERPSICHORE. Dr. Boozer was particularly helpful with the analysis in Sec. II B.

This work was supported by the U.S. Department of Energy Contract No. DE-AC02-76-CHO3073.

- ¹A. Reiman, G. Fu, S. Hirshman *et al.*, *European Physical Society Meeting on Controlled Fusion and Plasma Physics Research*, Maastricht, the Netherlands, 14–18 June 1999 (European Physical Society, Petit-Lancy, Switzerland, 1999).
- ²B. J. Braams, W. Jilge, and K. Lackner, *Nucl. Fusion* **26**, 699 (1986).
- ³H. P. Callaghan, P. J. McCarthy, and J. Geiger, *Nucl. Fusion* **39**, 509 (1999).
- ⁴G. H. Neilson, A. H. Reiman, M. C. Zarnstorff *et al.*, *Phys. Plasmas* **7**, 1911 (2000).
- ⁵P. Garabedian and L. P. Ku, *Phys. Plasmas* **6**, 645 (1999).
- ⁶S. P. Hirshman, W. I. van Rij, and P. Merkel, *Comput. Phys. Commun.* **43**, 143 (1986).
- ⁷J. Nührenberg and R. Zille, *Proceedings of the 5th International Workshop on Stellarators, Schloss Rinberg, 1984* (Commission of the European Communities, Brussels, 1984), EUR 9618EN 339.
- ⁸D. V. Anderson, A. Cooper, U. Schwenn, and R. Gruber, in *Proceedings of the Joint Varenna–Lausanne International Workshop on Theory of Fusion Plasmas* (Editrice Compositori, Bologna, 1988), p. 93.
- ⁹M. Yu. Isaev, M. I. Mikhailov, D. A. Monticello, H. E. Mynick, A. A. Subbotin, L. P. Ku, and A. H. Reiman, *Phys. Plasmas* **6**, 3174 (1999).
- ¹⁰W. H. Press, S. A. Teukolsky, W. T. Vetterling, and B. P. Flannery, *Numerical Recipes in FORTRAN 77* (Cambridge University Press, Cambridge, 1996), pp. 51ff.
- ¹¹S. P. Hirshman and J. Breslau, *Phys. Plasmas* **5**, 2664 (1998).
- ¹²N. Nakajima, M. Yokoyama, M. Okamoto, and J. Nührenberg, *Plasma Phys. Rep.* **23**, 460 (1997).
- ¹³A. H. Boozer (private communications, 1999).
- ¹⁴S. P. Hirshman (private communications, 1999).